Figure S1

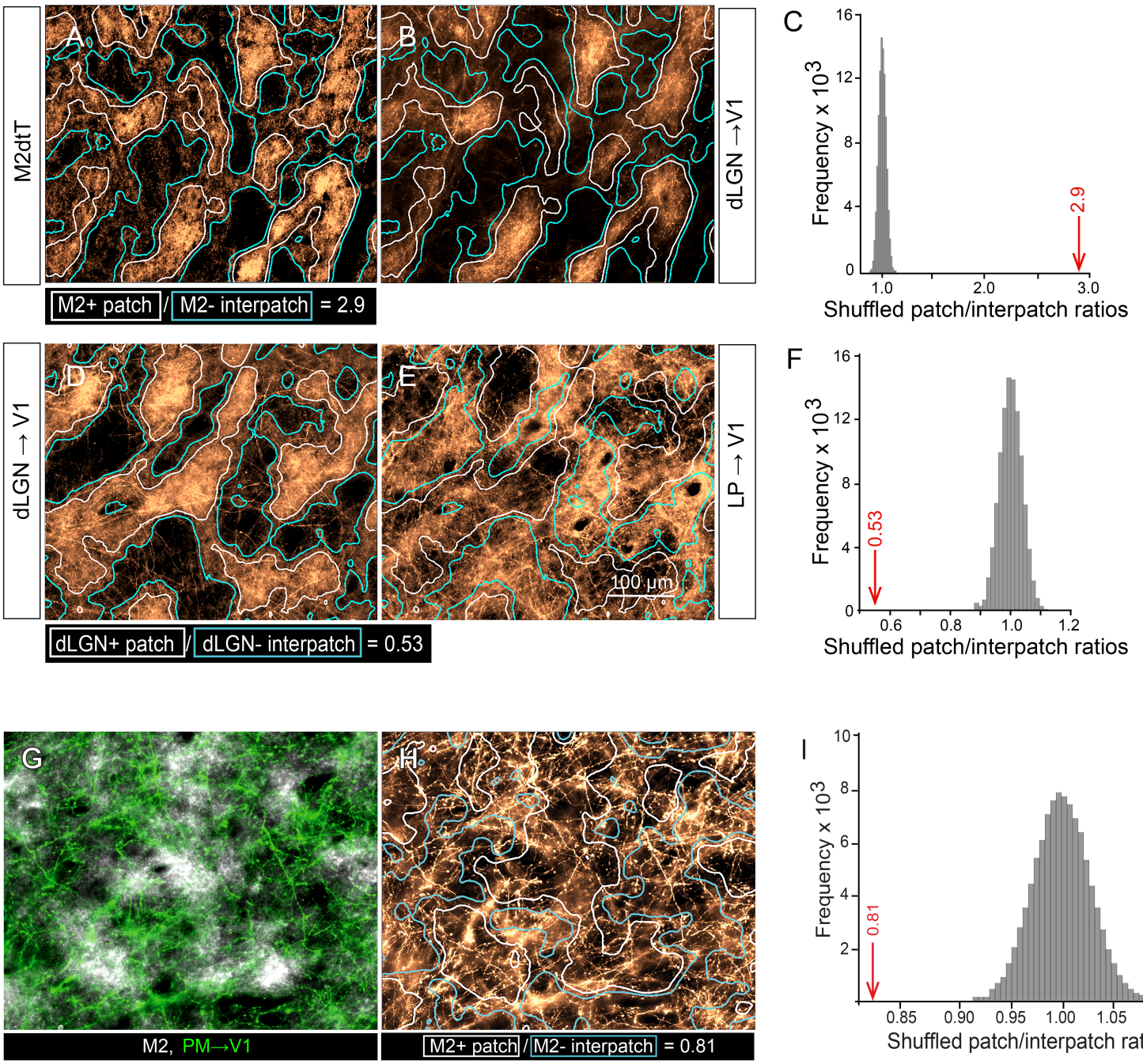
A
B
M2dtT
dLGN →V1
M2+ patch / M2- interpatch = 2.9
C
Frequency x 10^3
2.9
Shuffled patch/interpatch ratios
D
E
dLGN → V1
LP → V1
100 µm
dLGN+ patch / dLGN- interpatch = 0.53
F
Frequency x 10^3
0.53
Shuffled patch/interpatch ratios
G
H
M2, PM→V1
M2+ patch / M2- interpatch = 0.81
I
Frequency x 10^3
0.81
Shuffled patch/interpatch ratio

Figure S2

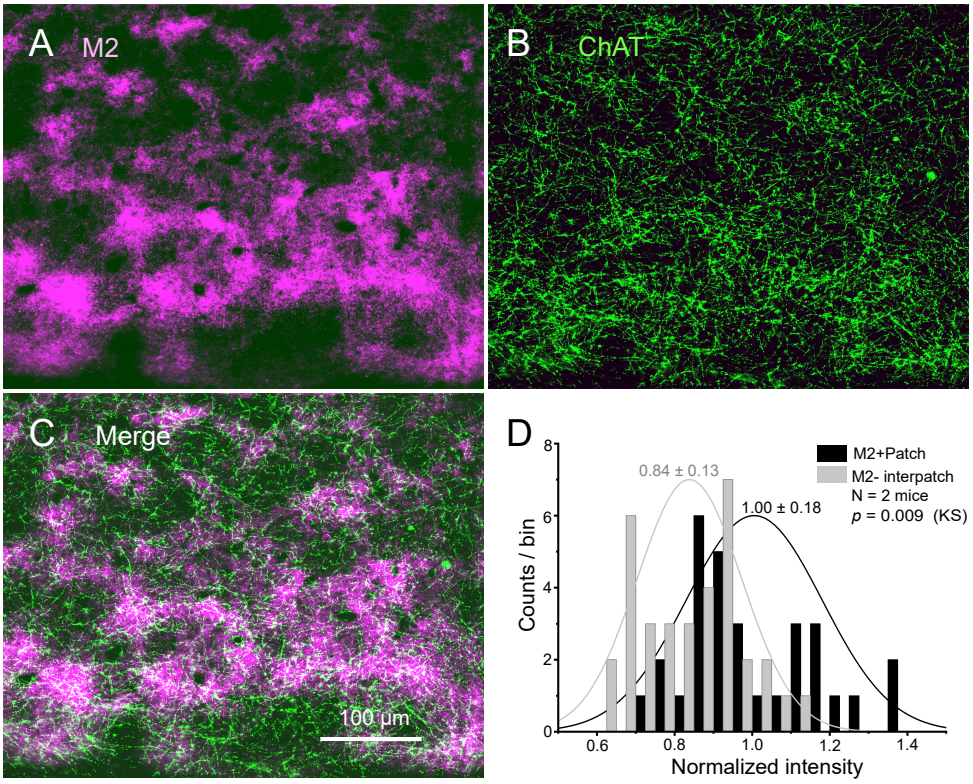
A
M2
B
ChAT
C
Merge
100 µm
D
M2+Patch
M2- interpatch
N = 2 mice
p = 0.009 (KS)
0.84 ± 0.13
1.00 ± 0.18
Counts / bin
Normalized intensity
0
2
4
6
8
0.6
0.8
1.0
1.2
1.4

Figure S3

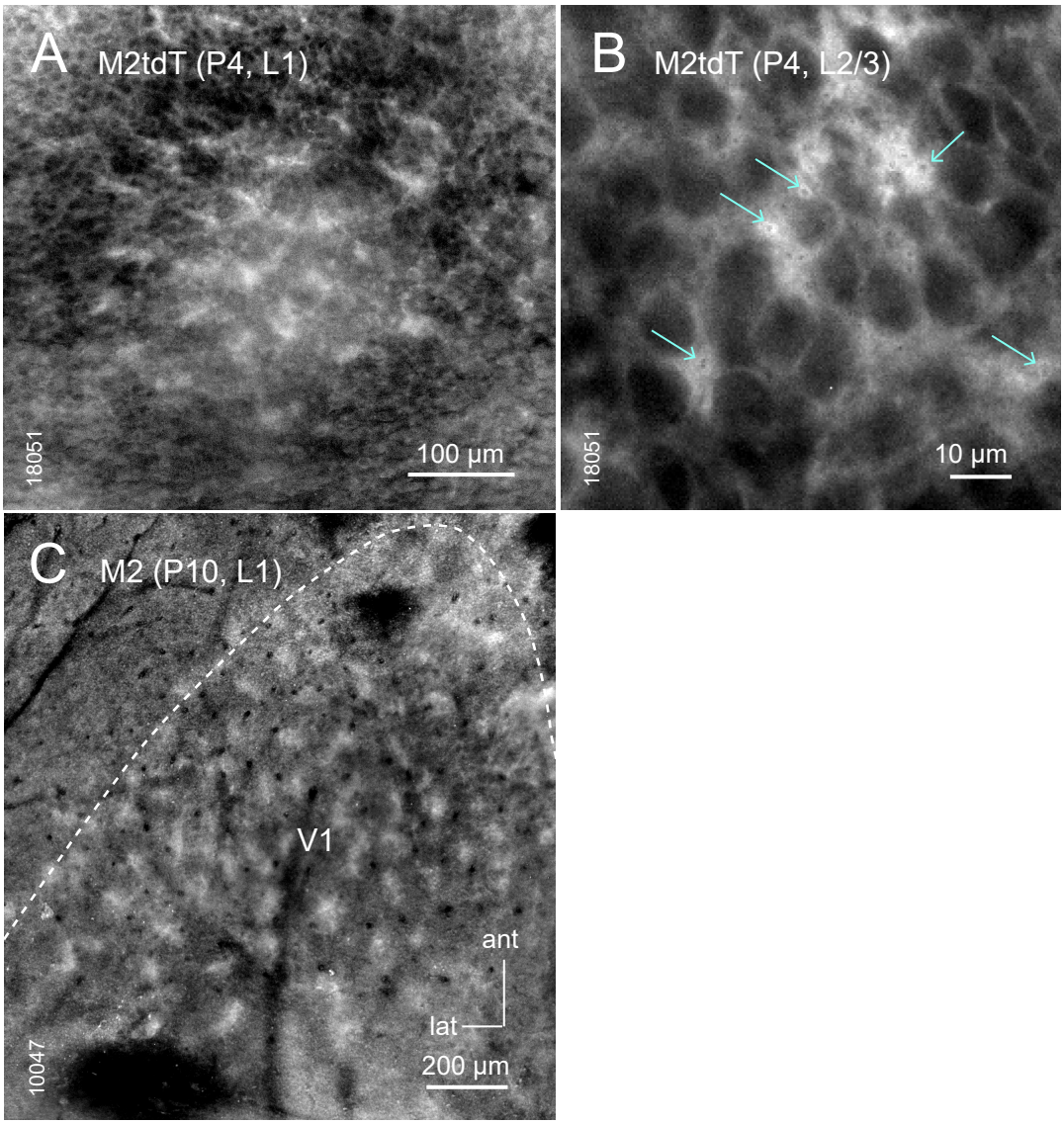
A
M2tdT (P4, L1)
18051
100 µm
B
M2tdT (P4, L2/3)
18051
10 µm
C
M2 (P10, L1)
V1
ant
lat
10047
200 µm

Figure S4

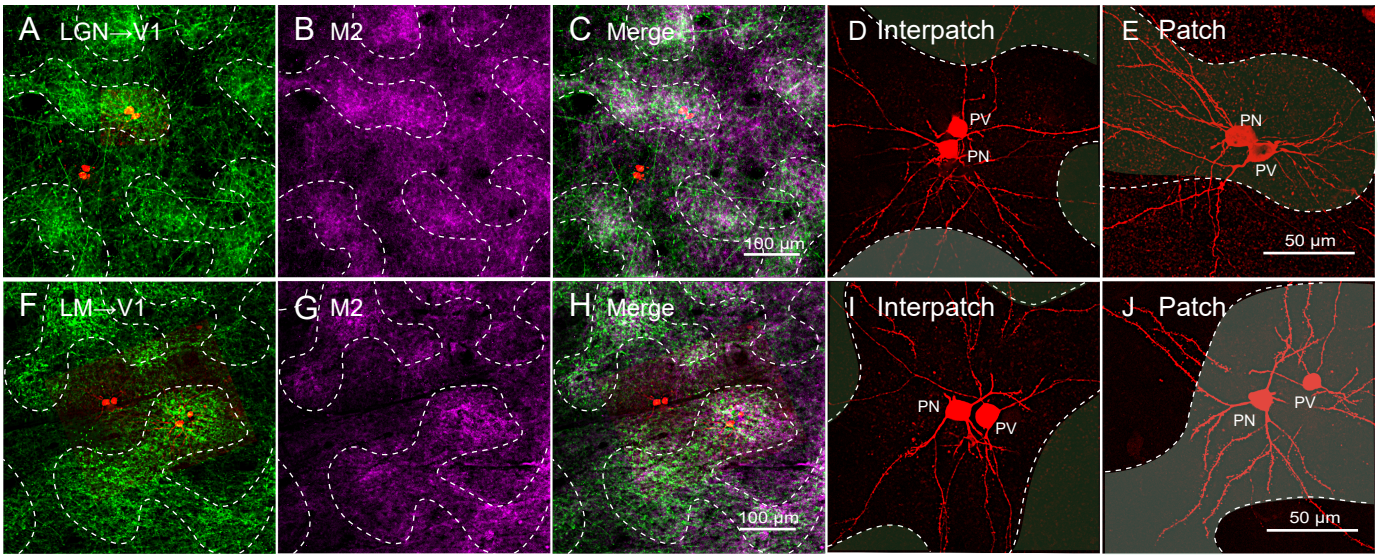
A LGN→V1
B M2
C Merge
100 µm
D Interpatch
PV
PN
E Patch
PN
PV
50 µm
F LM→V1
G M2
H Merge
100 µm
I Interpatch
PN
PV
J Patch
PV
PN
50 µm

Figure S5

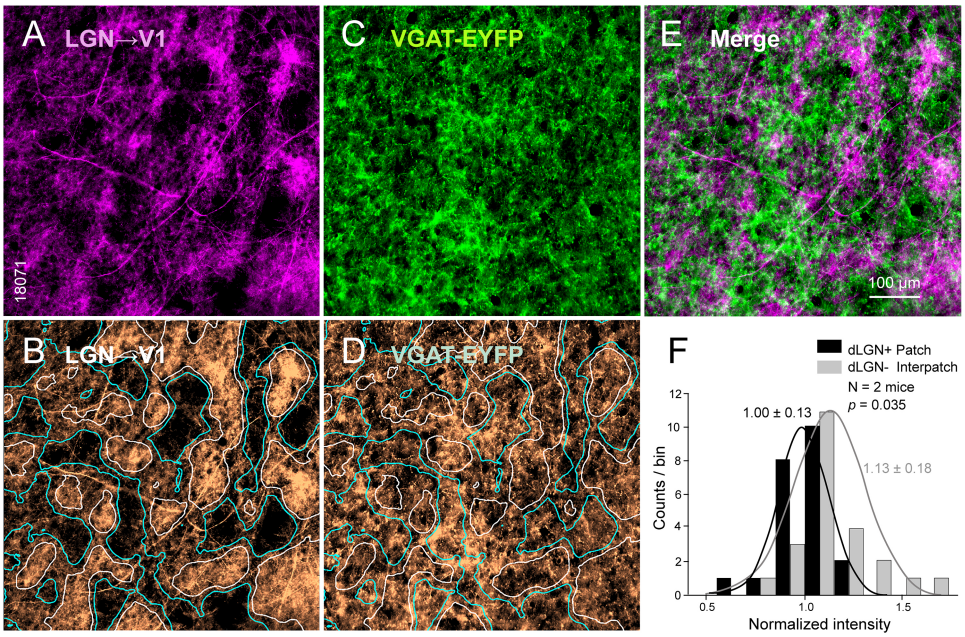
A LGN→V1
C VGAT-EYFP
E Merge
18071
100 µm
B LGN→V1
D VGAT-EYFP
F
dLGN+ Patch
dLGN- Interpatch
N = 2 mice
p = 0.035
1.00 ± 0.13
1.13 ± 0.18
Counts / bin
Normalized intensity

G

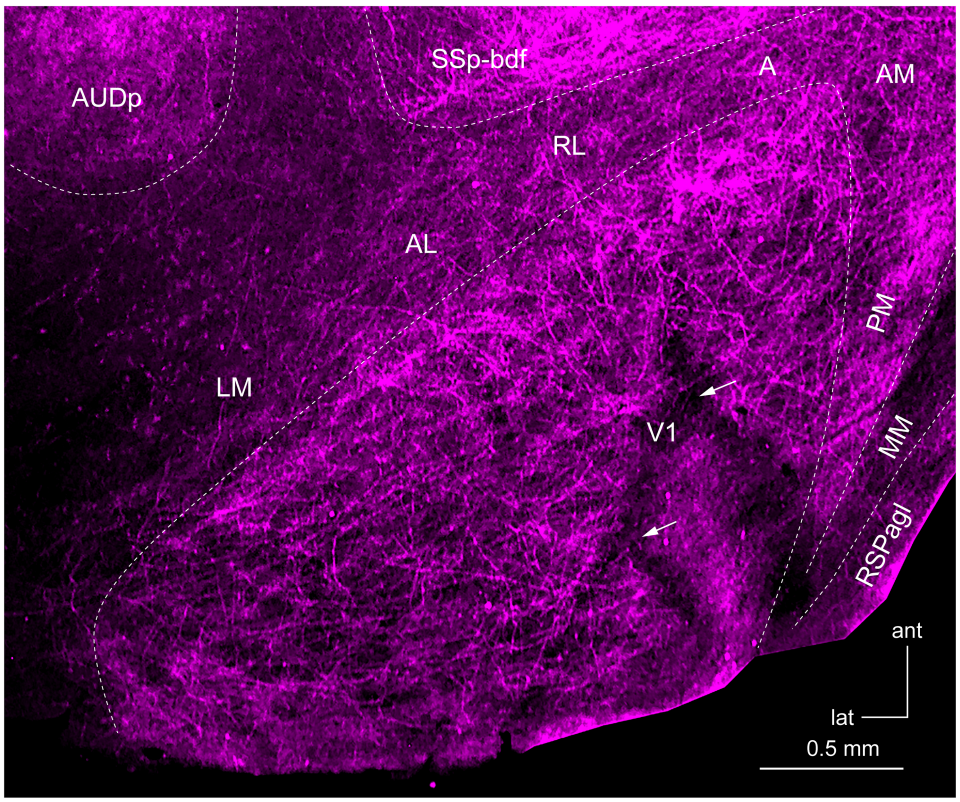
AUDp
SSp-bdf
A
AM
RL
AL
PM
LM
V1
MM
RSPagl
ant
lat
0.5 mm

Figure S6

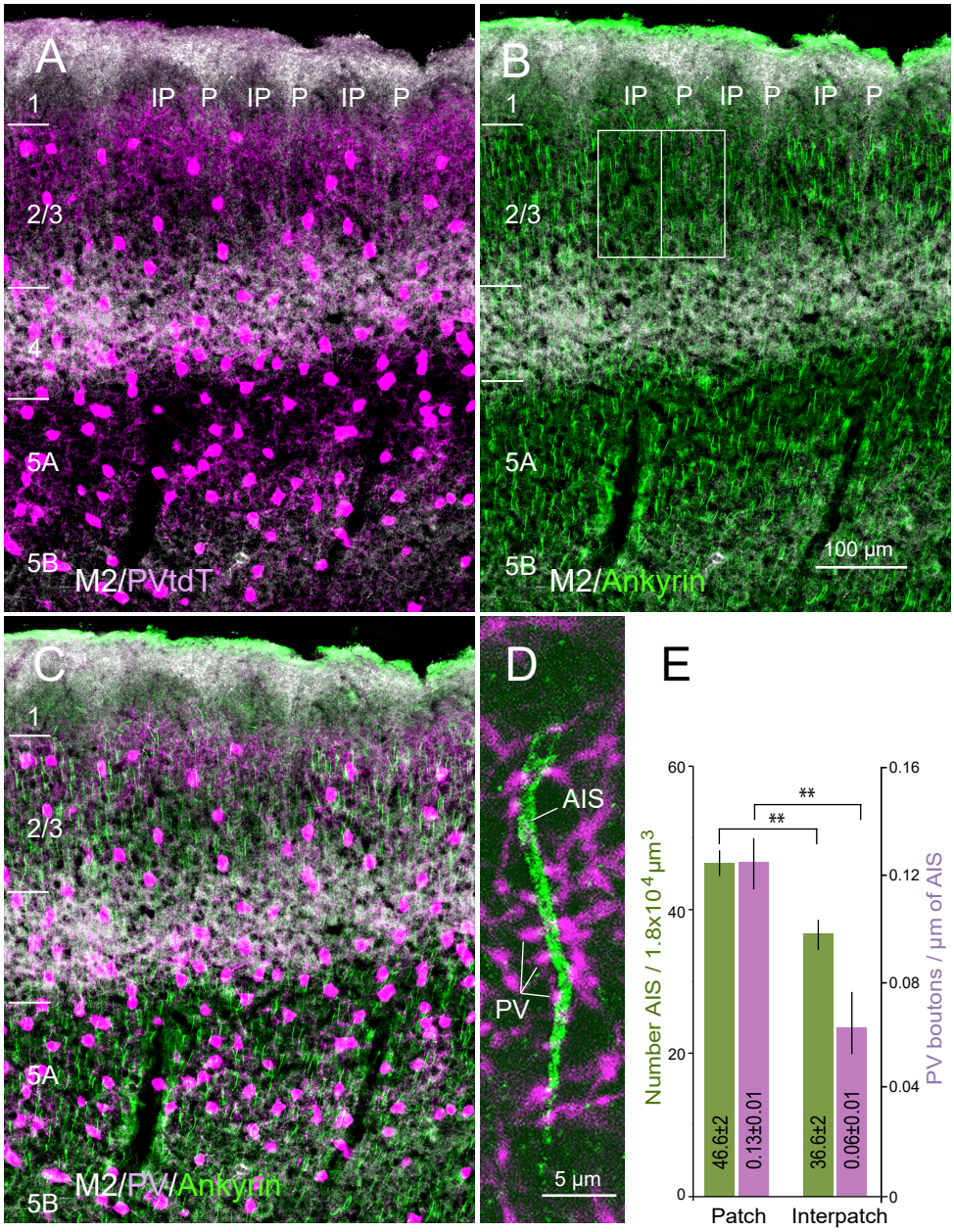
A
1
IP P IP P IP P
2/3
4
5A
5B
M2/PVtdT
B
1
IP P IP P IP P
2/3
5A
5B
M2/Ankyrin
100 µm
C
1
2/3
5A
5B
M2/PV/Ankyrin
D
AIS
PV
5 µm
E
Number AIS / 1.8x10^{4}µm^3
PV boutons / µm of AIS
60
40
20
0
0.16
0.12
0.08
0.04
0
**
**
46.6±2
0.13±0.01
36.6±2
0.06±0.01
Patch
Interpatch

Figure S7

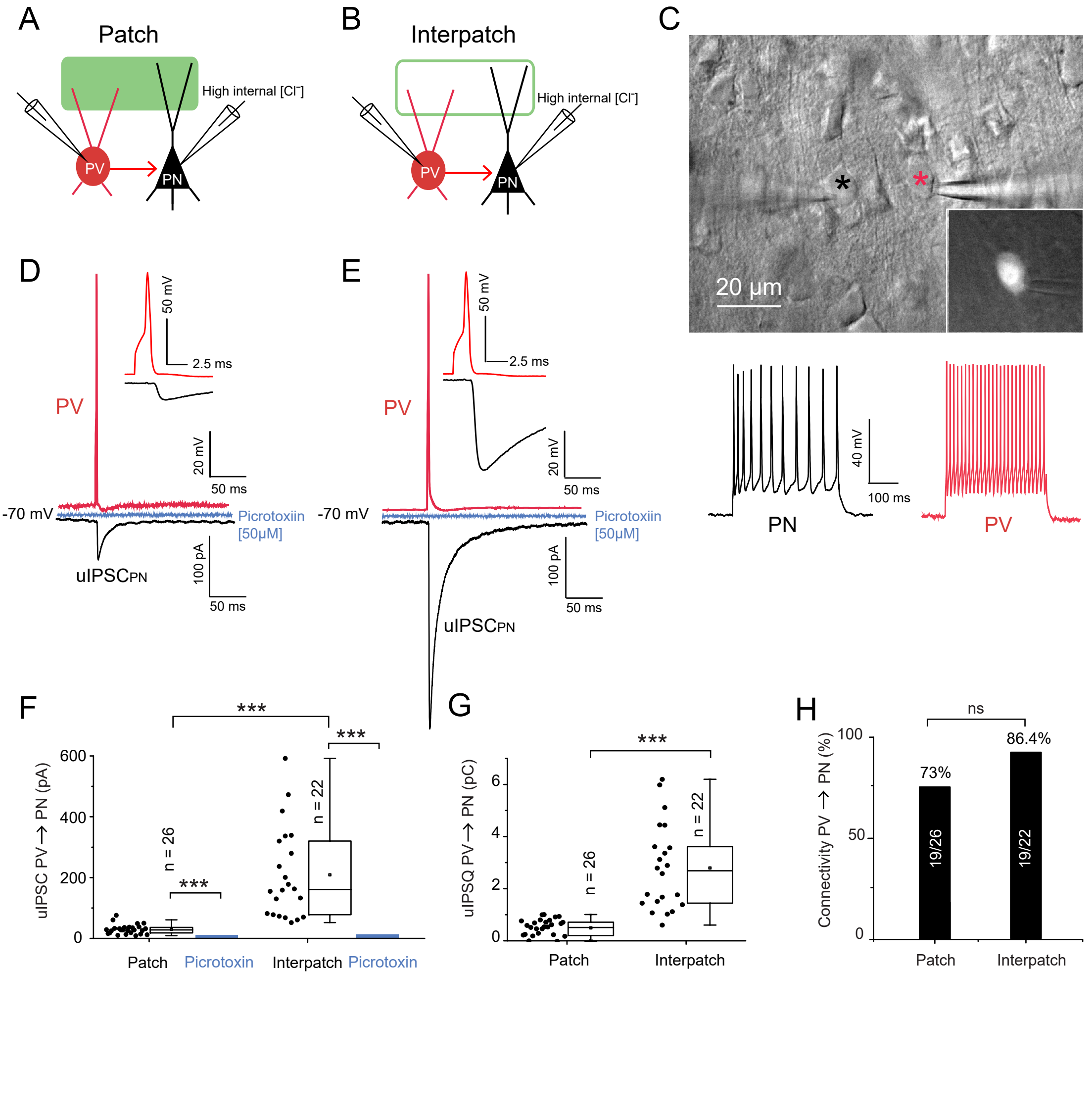
A
Patch
High internal [Cl⁻]
PV
PN
B
Interpatch
High internal [Cl⁻]
PV
PN
C
20 µm
D
PV
50 mV
2.5 ms
20 mV
50 ms
-70 mV
Picrotoxiin [50µM]
uIPSCPN
100 pA
50 ms
E
PV
50 mV
2.5 ms
20 mV
50 ms
-70 mV
Picrotoxiin [50µM]
uIPSCPN
100 pA
50 ms
40 mV
100 ms
PN
PV
F
***
***
***
uIPSC PV→PN (pA)
600
400
200
0
n = 26
n = 22
Patch
Picrotoxin
Interpatch
Picrotoxin
G
***
uIPSQ PV→PN (pC)
6
4
2
0
n = 26
n = 22
Patch
Interpatch
H
ns
Connectivity PV→PN (%)
100
50
0
73%
86.4%
19/26
19/22
Patch
Interpatch

SUPPLEMENTAL FIGURE LEGENDS

Figure S1. Intensity contour maps of dLGN→V1,LP→V1, and PM→V1 projections to L1, Related to Figures 1 and 2. (A, B) Distribution of fluoresence intensity of M2tdT expression (A) and dLGN→V1 projections (B) (same section as in Figures 1A, B). Patches are outlined by white lines (top 33% quantile of M2tdT fluorescence intensity), interpatches by cyan lines (bottom 33% quantile of M2tdT intensity). (C) Distribution of patch/interpatch ratios for each of 10^5 randomly shuffled iterations of pixel values (see Methods) from (B). Mean patch/interpatch ratio of dLGN axons (red arrow) is significantly higher than chance, indicating denser dLGN→V1 projections in patches. (D, E) Interdigitating maps of dLGN→V1 (D) and LP→V1 (E) projections (same section as in Figures 1I, J). Patches (white lines) and interpatches (cyan lines) determined by density of dLGN axons in (D). (F) Distribution of patch/interpatch ratios for 10^5 iterations of randomly shuffled pixel values from (E). Patch/interpatch ratio of LP→V1 axons density (red arrow) is significantly lower than chance, indicting stronger input to interpatches. (G) Overlay of PM→V1 axons (green) and M2 immunostaining (white). Same images as in Figures 2C, E. (H) M2+ patches and M2- interpatches are delineated by white and cyan lines, respectively, based on the top and bottom 33% quantiles of M2 intensity from Figures 2C, S1G. (I) Distribution of patch/interpatch ratios for each of 10^5 iterations of randomly shuffled pixel values in Figure 2E, for M2+ patches and M2- interpatches shown in (B). Mean patch/interpatch ratio (red arrow) of PM→V1 density in M2+ patches is significantly lower than chance.

Figure S2. Cholinergic axons preferentially innervate M2 patches in L1 of V1, Related to Figures 1 and 2. (A, B) Tangential section through V1 showing double immunofluorescence of M2+ patches (magenta) and ChAT axons (green) in L1. (C) Overlay of (A) and (B). (D) Normalized (to patches) fluorescence intensity showing stronger ChAT expression in M2+ patches. KS test, mean ± SD.

Figure S3. Development of M2 patches in L1 of V1, Related to Figures 1 and 2. (A, B) Tangential section through V1 showing patchy expression of M2 in L1 of 4 day-old Chrm2tdT mouse (A). At higher magnification membrane-bound M2 expression in L2/3 shows rings of crossectioned dendritic bundles (arrows) occupying the spaces between unstained cells bodies (B). (C) Patchy pattern of M2 immunostaining in L1 of V1 of 10 day-old C57BL/6J mouse.

Figure S4. Recordings of L2/3 PVs and PNs in patches and interpatches of V1, Related to Figure 3. (A-C) Confocal z-stack (200 µm) of tangential slice through L1-2 of V1 showing Alexa

594 hydrazide-filled pairs of PVs and PNs (red) aligned with Venus-expressing patch of LGN→V1 input to L1 (green) and Venus-negative interpatch. (B) Same slice as in (A) labeled with an antibody against M2. (C) Overlay of (A) and (B). (D) Alexa 594 hydrazide-filled interpatch-PVs and -PNs (same as in A) showing that apical dendrites branch preferentially in interpatches (unshaded regions). (E) Patch-PVs and -PNs (same as in (A) showing that dendrites preferentially branch in patches (shaded regions). (F-J) Same format as (A-E), except that the Venus-expressing patches represent LM→V1 inputs. Note that similar to LGN→V1 projections, LM inputs overlap with M2 patches (H).

Figure S5. Clustering of VGAT expression and PVtdT fibers in V1, Related to Figure 6. (A-E) Tangential section through L1B of V1 of VGAT-EYFP mouse. (A, B) Patchy dLGN→V1 input to L1 labeled by tracing with AAV2/1hSyn.tdTomato.WPRE.bGH (A) and corresponding contour map of dLGN+ patches (white lines) and dLGN- interpatches (cyan lines) (B). (C-E) Patchy VGAT-EYFP expression (C) and corresponding contour map (D) showing preferential labeling of interpatches (cyan lines). (E) Overlay of A and C showing interdigitating patterns of dLGN→V1 (magenta) projections and VGAT (green). (F) Normalized (to patches) fluorescence intensity of VGAT-EYFP in interpatches. Mean ± SD, KS test, N = number of mice. (G) Tangential section through L1 (70 µm below pial surface) of V1 of PVtdT mouse, showing clusters of tdT labeled dendrites and axons. Arrows points to branched blood vessel. Lateromedial area (LM), anterolateral area (AL), rostrolateral area (RL), anteromedial area (AM), posteromedial area (PM), Mediomedial area (MM), restrosplenial agranular area (RSPagl), primary auditory area (AUDp), somatosensory barrel cortex (SSp-bdf).

Figure S6. Ankyrin G immunolabeled axon initial segments (AIS) of L2/3 PNs aligned with M2 patches are densely innervated by axo-axonic PV boutons, Related to Figure 6. (A) M2 immunolabeling (white) in parasagittal section through V1 of PVtdT (magenta) mouse. Patch (P). Interpatch (IP). (B) Same section as in (A) showing Ankyrin G immunolabeling of AIS (green) and M2 expression (white). Boxes indicate regions in L2/3 aligned with patches and interpatches in which PV+ boutons in putative contact with AIS were counted. (C) Overlay of (A) and (B). (D) Confocal image showing putative contacts of PV boutons (magenta) with Ankyrin G labeled AIS (green). (E) Number of AIS in L2/3 vertically aligned with patches and interpatches in L1. Length density of putative PV contacts with L2/3 AIS in patches and interpatches. Paired t-test, ** $p < 0.01$.

Figure S7 Distinct strengths of inhibition in patches and interpatches, Related to Figure 7. (A, B) Diagram of dual whole cell patch clamp recordings in coronal slices of V1 showing unitary uIPSC in L2/3 PNs elicited by presynaptic action potentials from L2/3 PVs. Patches (solid green) and interpatches (green outline) were identified by tracing of dLGN→V1 projections to L1 with AAV2/9.CAG.ChR2.Venus.WPRE.SV40. Recordings from PNs were made with high [Cl^-] internal solution to shift equilibrium potential of IPSCs to 0 mV and record IPSCs at -70 mV as inward currents. Recordings from PVs were made with K-gluconate internal solution. (C) IR-DIC image showing paired recordings from L2/3 PN (black *, regular spiking shown below), and PV (red *, tdT expression shown in inset, fast spiking response below). (D, E) Recordings from synaptically connected PVs and PNs in patch (D) and interpatch (E). Spike fired by current injection in presynaptic PV (red trace). Voltage clamp recording of uIPSCs from postsynaptic PNs (black). Note that uIPSCs are larger in interpatches (E) than patches (D). uIPSCs are blocked by bath application of Picrotoxin (blue). The insets in (D) and (E) show that uIPSCs follow presynaptic spikes with delays consistent with monosynaptic connections. (F) Box plots of uIPSC recorded from PNs in patches and interpatches. Bath application of Picrotoxin abolished uIPSCs (***p < 0.001, paired t-test). uIPSCs in interpatches are larger (***p < 0.001). (G) The total unitary inhibitory charge (IPSQ) is larger (***p < 0.001, two-sample t-test) in interpatches than patches. (H) The percentage of total of recorded pairs of PV→PN connections in patches is slightly (but not significantly, Chi square test) smaller in patches than interpatches.